APPENDIX A: TEST CASE DESCRIPTION AND SYSTEM DATA

To verify the effectiveness of the proposed coordination framework and model, several EVCSs with distributed PV or BESS in constrained PDN and UTN are investigated. In this paper, the 12-node UTN and the modified IEEE 33-bus three-phase PDN are used for our studies as displayed in Fig. A1. The parameters of UTN and PDN are provided in [F1],[F2] (See APPENDIX F). The origin-destination (O-D) pairs and the corresponding traffic demand forecast value of UTN are from [F2] as listed in Table A.I, where the standard deviation of traffic demand forecast error is set as 5% of the expected value. The time cost coefficients of free and delay travel are set as 0.2$/min and 0.4$/min, respectively. The individual EV capacity is generated from 40kWh to 64kWh, randomly. The installed PV capacities of EVCSs are range from 200kW to 250kW, and the installed local BESS capacities are range from 150kWh to 250kWh. The energy procurement price from PDN is displayed in Fig. A2, and the energy sale price to PDN is fixed as 0.014$/kWh. The Spearman correlation coefficients between renewables and electric load are revised from [F3] and [F4].

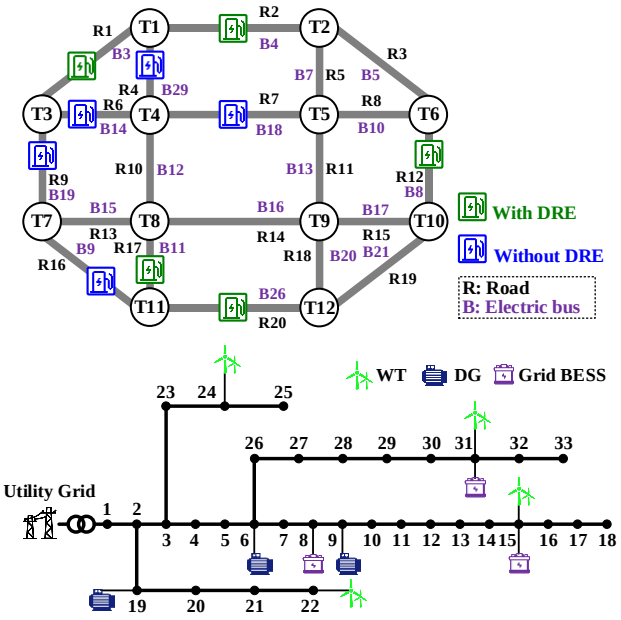

Fig. A1. UTN and PDN topology and their correlations

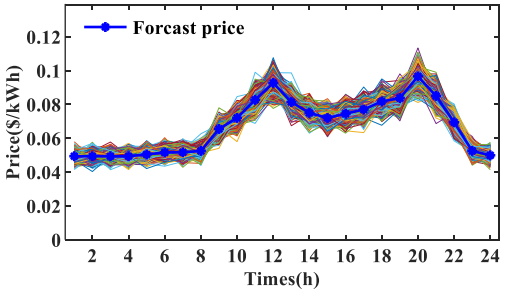

Fig. A2. Forecast PDN electricity price and its uncertain scenarios

TABLE A.I
O-D PAIRS AND TRAFFIC DEMAND IN UTN

O-D pairs	1-12	2-7	3-11	6-3	7-6	10-1
Traffic demand	600	800	500	500	800	600

TABLE A.II
THE PARAMETERS OF DGS

DG	Bus	$P^{dg,min}$ / $P^{dg,max}$	*RU*	*RD*	θ^{min} / θ^{max}	b_2	b_1
1	6	0/0.86	0.52	0.52		$9*10^{-3}$	58
2	9	0/0.76	0.38	0.38	0/0.9	$10*10^{-3}$	60
3	19	0/0.98	0.72	0.72		$11*10^{-3}$	62

$P^{dg,max}$, $P^{dg,min}$: maximum/minimum power output (MW)
RU, RD: maximum up/down ramp rate (MW/h)
θ^{max}, θ^{min}: maximum/minimum power factor
Generation cost: $b_2P^2 + b_1P$ ($), where $b_2(\$/MW^2)$, $b_1(\$/MW)$

TABLE A.III
THE PARAMETERS OF GRID BESSS

BESS	Bus	E^{max}	E^{min}	$P^{ch,max}$	$P^{dis,max}$	η^{ch} / η^{dis}
1	8	0.46	0.046	0.17	0.17	
2	15	0.52	0.052	0.18	0.18	0.9
3	31	0.42	0.042	0.16	0.16	

$P^{ch,max}$, $P^{dis,min}$: maximum charging/discharging power (MW)
E^{max}, E^{min}: maximum/minimum energy storage (MWh)
η^{ch}, η^{dis}: Charging/discharging efficiency
Degradation cost: $c_0(P^{ch}\eta^{ch} + \frac{P^{dis}}{\eta^{dis}})$

In addition, the PDN contains three DGs, three grid BESSs and four WTs, which locations are also displayed in Fig. A1. The detailed parameters of DGs and grid BESSs are listed in Table A.II and Table A.III, and the rated power of each WT is 160 kW. The degradation costs of grid BESSs are provided in [F2]. The WT and load forecast data are offered in [F5] and [F2], respectively. The energy purchase price from upstream grid (UG) for DSO is the same as the PDN electricity price, which value is displayed by the blue line in Fig. A2. The price for the reactive power purchased from external ancillary service market and local flexible recourse are set as 20% of the UG electricity price. The reserve prices of local flexible recourses are from [F6]. The secure voltage range is from 0.9 p.u. to 1.1 p.u.. The maximum VUR is set as 3%, which can be adjusted according to different operation requirements by DSO.

APPENDIX B: DETAILED EV CHARGING LOAD ASSIGNMENT MODEL

The EV charging load assignment is implemented by TSO through solving the traffic flow assignment problem (TAP), which is formulated based on Nesterov model using primal-dual method [F1]. The EV charging expense is accommodated in the objective function through introducing the time-price factor for monetizing the travel time cost. Thus, the objective function of EV charging load assignment problem is to minimize the total travel and charging costs as follow:

$$\min F_{UTN}^{TSO} = F_{UTN}^{free}(\boldsymbol{x}^{ch}, \boldsymbol{x}^{non}) + F_{UTN}^{jam}(\boldsymbol{x}^{ch}, \boldsymbol{x}^{non}) + F_{EV}^{ch}(\boldsymbol{P}^{EV}) \quad \text{(B1)}$$

$$F_{UTN}^{free} = \sum_t \sum_a \lambda^{free} t_a^0 (x_{a,t}^{ch} + x_{a,t}^{non}), \forall a \in T_A^{free} \quad \text{(B2)}$$

$$F_{UTN}^{jam} = \sum_t \sum_a \lambda^{jam} (t_a^0 + t_{a,t}^{del})(x_{a,t}^{ch} + x_{a,t}^{non}), \forall a \in T_A^{jam} \quad \text{(B3)}$$

$$F_{EV}^{ch} = \sum_{t\in\mathcal{T}} \sum_{h\in\Omega} \lambda_{h,t}^{ch} P_{h,t}^{ev} \tag{B4}$$

where $\boldsymbol{x^{ch}} = \{x_{a,t}^{ch}, \forall a, \forall t\}$ and $\boldsymbol{x^{non}} = \{x_{a,t}^{non}, \forall a, \forall t\}$ means the traffic flow vectors of charging and non-charging vehicles. $\boldsymbol{P^{EV}} = \{P_{h,t}^{ev}, \forall h, \forall t\}$ is the assigned charging power vector at EVCSs. The objective function (B1) contains three terms as expressed in (B2) - (B4), which are travel time cost on non-congested roads, travel time cost on congested roads and EV charging expense, respectively. λ^{free} and λ^{jam} indicates the time-price factors of non-congestion and congestion. t_a^0 is the free travel time of road *a*. $t_{a,t}^{del}$ is equal to the dual variable of (B6), which is regarded as the traffic delay time when occurring the road congestion. $\lambda_{h,t}^{ch}$ is the charging price of EVCS *h*. The UTN operation constraints are listed as follow:

$$x_{a,t} = x_{a,t}^{ch} + x_{a,t}^{non}, \forall a, \forall t \tag{B5}$$

$$x_{a,t} \le c_a : \lambda_{a,t}, \forall a, \forall t \tag{B6}$$

$$\sum\nolimits_{k\in K_{rs}} f_{rs,k,t}^{ch} = \gamma_1\gamma_2 D_{rs,t}^{UTN} : \pi_{rs,t}^{ch}, \forall rs, \forall t \tag{B7}$$

$$\sum\nolimits_{k\in K_{rs}} f_{rs,k,t}^{non} = (1-\gamma_1\gamma_2) D_{rs,t}^{UTN} : \pi_{rs,t}^{non}, \forall rs, \forall t \tag{B8}$$

$$f_{rs,k,t}^{ch} \ge 0,\ f_{rs,k,t}^{non} \ge 0, \forall k \in K_{rs}, (r,s) \in \boldsymbol{OD}, \forall t \tag{B9}$$

$$x_{a,t}^{ch} = \sum\nolimits_{rs} \sum\nolimits_{k} \Lambda_{a,k}^{rs} \cdot f_{rs,k,t}^{ch} : \mu_{a,t}^{ch}, \forall rs, k, a, t \tag{B10}$$

$$x_{a,t}^{non} = \sum\nolimits_{rs} \sum\nolimits_{k} \Lambda_{a,k}^{rs} \cdot f_{rs,k,t}^{non} : \mu_{a,t}^{non}, \forall rs, k, a, t \tag{B11}$$

$$\lambda_{a,t} \ge 0, \forall a, \forall t \tag{B12}$$

$$\pi_{rs,t}^{ch} - \sum\nolimits_{a} ([\Lambda_{a,k}^{rs}]^T \cdot \mu_{a,t}^{ch}) \le 0, \forall rs, \forall t \tag{B13}$$

$$\pi_{rs,t}^{non} - \sum\nolimits_{a} ([\Lambda_{a,k}^{rs}]^T \cdot \mu_{a,t}^{non}) \le 0, \forall rs, \forall t \tag{B14}$$

$$\mu_{a,t}^{ch} - \lambda_{a,t} = t_a^0, \forall a \in T_A \tag{B15}$$

$$\mu_{a,t}^{non} - \lambda_{a,t} = t_a^0, \forall a \in T_A \tag{B16}$$

$$\begin{aligned} &\gamma_1\gamma_2 \sum\nolimits_t \sum\nolimits_{rs} \pi_{rs,t}^{ch} D_{rs,t}^{UTN} + (1-\gamma_1\gamma_2) \sum\nolimits_t \sum\nolimits_{rs} \pi_{rs,t}^{non} D_{rs,t}^{UTN} \\ &= \sum\nolimits_t \sum\nolimits_a [t_a^0 (x_{a,t}^{ch} + x_{a,t}^{non}) + c_a \lambda_{a,t}] \end{aligned} \tag{B17}$$

$$\sum\nolimits_h f_{h,t}^{assi} = \gamma_1\gamma_2 \sum\nolimits_{rs} D_{rs,t}^{UTN}, \forall t \tag{B18}$$

$$0 \le f_{h,t}^{assi} \le N_h^{port}, \forall h \in \Omega \tag{B19}$$

$$f_{h,t}^{assi} \le \sum\nolimits_{rs} \sum\nolimits_{k} (X_{k,h}^{rs} \cdot f_{rs,k,t}^{ch}), \forall h, \forall t \tag{B20}$$

$$f_{rs,k,t}^{ch} \le \sum\nolimits_{h} ([X_{k,h}^{rs}]^T \cdot f_{h,t}^{assi}), \forall rs, k, t \tag{B21}$$

$$P_{h,t}^{ev} = \Delta p_{h,t} \cdot f_{h,t}^{assi}, \forall h \in \Omega \tag{B22}$$

The road traffic flow constraints are imposed in (B5-6), where $x_{a,t}$ and c_a are the traffic flow and road capacity of road *a*, respectively. The relationship of the path flow and traffic demand is indicated in (B7-9), where $f_{rs,k,t}^{ch}$ and $f_{rs,k,t}^{non}$ are the path flow of charging and non-charging vehicles on path *k* of O-D pair *rs*. γ_1 is the percentage of EVs with respect to all vehicles, and γ_2 is the proportion of charging EVs with respect to all EVs. $D_{rs,t}^{UTN}$ is the traffic demand of O-D pair *rs*. (B10-11) impose the relation of road flow and path flow, where $\boldsymbol{\Lambda} = \{\Lambda_{a,k}^{rs}, \forall rs, a, k\}$ is the corresponding road-path correlation matrix. Eq. (B12-17) constrain the dual variables of original constraints, where $\pi_{rs,t}^{ch}$, $\pi_{rs,t}^{non}$, $\mu_{a,t}^{ch}$ and $\mu_{a,t}^{non}$ are the dual variables of (B7-8) and (B10-11), respectively. $[.]^T$ means matrix transposition. Eq. (B17) shows the strong dual condition, which guarantees the same solution for the original and dual problems. Eq. (B18) means all the charging EVs are assigned to EVCSs, where $f_{h,t}^{assi}$ is the assigned EV flows to EVCS *h*. The assigned EV flows cannot exceed the EV ports of EVCSs as illustrated in (B19). Eq. (B20-21) relate the EV flows assigned to an EVCS and traffic flow through the corresponding road, where the correlation matrix $\boldsymbol{X} = \{X_{k,h}^{rs}, \forall rs, k, h\}$ relates the EVCS location to the travel path. The charging load assignment for an EVCS is proportional to assigned EV flows, as shown in (B22).

Thus, the EV charging load assignment problem in UTN is formulated as

$$\begin{aligned} &\textit{minimize } F_{UTN}^{TSO}(\boldsymbol{x^{UTN}}, \boldsymbol{x^{dual}}, \boldsymbol{f^{CS}}, \boldsymbol{P^{EV}}) \\ &\textit{s.t. } \text{(B2)-(B22)} \end{aligned} \tag{B23}$$

where $\boldsymbol{x^{UTN}}$ denotes the UTN decision variable vector; $\boldsymbol{x^{dual}}$ means the dual variable vector in TAP; $\boldsymbol{f^{CS}}$ and $\boldsymbol{P^{EV}}$ indicate the EV allocation variable vectors regarding traffic flow and charging load.

APPENDIX C: DETAILED OPERATION CONSTRAINTS FOR DGS AND BESSS

- Constraints of DGs

$$P_i^{dg,\min} + R_{i,t}^{dn} \le P_{i,t}^{dg} \le P_i^{dg,\max} - R_{i,t}^{up}, \forall i \in \boldsymbol{I}_g, t \tag{C1}$$

$$-\mathrm{RD}_i \Delta t \le P_{i,t}^{dg} - P_{i,t-1}^{dg} \le \mathrm{RU}_i \Delta t, \forall i \in \boldsymbol{I}_g, t \tag{C2}$$

$$0 \le R_{i,t}^{up} \le RU_i \Delta t, 0 \le R_{i,t}^{dn} \le RD_i \Delta t, \forall i \in \boldsymbol{I}_g, t \tag{C3}$$

$$P_{i,t}^{dg} \cdot \theta_i^{\min} \le Q_{i,t}^{dg} \le P_{i,t}^{dg} \cdot \theta_i^{\max}, \forall i \in \boldsymbol{I}_g, t \tag{C4}$$

$$P_{i,t}^{dg} = \sum\nolimits_{\phi} P_{i,\phi,t}^{dg}, Q_{i,t}^{dg} = \sum\nolimits_{\phi} Q_{i,\phi,t}^{dg}, \forall i, t \tag{C5}$$

Eq. (C1) constrains the power output of DGs, where $P_i^{dg,\max}$, $P_i^{dg,\min}$ indicate the maximum and minimum power output; $R_{i,t}^{up}$, $R_{i,t}^{dn}$ are the up/down reserve provided by DG *i*. The ramping limitation of DGs is illustrated in (C2). The provided reserve cannot exceed the ramping limitation as shown in (C3). The reactive power of DGs is limited by (C4), where $\theta_i^{\max}$ and $\theta_i^{\min}$ are the maximum and minimum power factors. The three-phase active and reactive power of DGs are expressed in (C5).

- Constraints of grid BESSs

$$E_{i,t}^{ess} = E_{i,t-1}^{ess} + (P_{i,t}^{ch}\eta_i^{ch} - P_{i,t}^{dis} / \eta_i^{dis})\Delta t, \forall i \in \boldsymbol{I}_s, t \tag{C6}$$

$$E_i^{ess,\min} \le E_{i,t}^{ess} \le E_i^{ess,\max}, \forall i \in \boldsymbol{I}_s, t \tag{C7}$$

$$0 \le P_{i,t}^{ch} + R_{i,t}^{dn} \le P_{i,t}^{ch,\max}, \forall i \in \boldsymbol{I}_s, t \tag{C8}$$

$$0 \le P_{i,t}^{dis} + R_{i,t}^{up} \le P_{i,t}^{dis,\max}, \forall i \in \boldsymbol{I}_s, t \tag{C9}$$

$$-\alpha_i^{\max} \left| P_{i,t}^{ch} - P_{i,t}^{dis} \right| \le Q_{i,t}^{ess} \le \alpha_i^{\max} \left| P_{i,t}^{ch} - P_{i,t}^{dis} \right|, \forall i \in \boldsymbol{I}_s, t \tag{C10}$$

$$P_{i,t}^{ch} = \sum\nolimits_{\phi} P_{i,\phi,t}^{ch}, P_{i,t}^{dis} = \sum\nolimits_{\phi} P_{i,\phi,t}^{dis}, \forall i \in \boldsymbol{I}_s, t \tag{C11}$$

$$Q_{i,t}^{ess} = \sum\nolimits_{\phi} Q_{i,\phi,t}^{ess}, \forall i \in \boldsymbol{I}_s, t \tag{C12}$$

Eq. (C6-7) indicates the charging state of grid BESSs, where η_i^{ch} and η_i^{dis} are the charging & discharging efficiency;

$E_i^{ess,\max}$ and $E_i^{ess,\min}$ are the maximum & minimum energy storage of grid BESSs. The reserve provided by grid BESSs is constrained by (C8-9), where $P_{i,t}^{ch,\max}$ and $P_{i,t}^{dis,\max}$ means the maximum charging & discharging power. Eq. (C10) limits the reactive power from grid BESSs, where $\alpha_i^{\max}$ is the maximum power factor. Eq. (C11-12) express the three-phase active and reactive power.

APPENDIX D: PROOF FOR PROPOSITION 1

Here, we derive the sensitivity matrixes of system variables (i.e., line flow and nodal voltage) respond to nodal power, which express the influences of nodal power on line flow and nodal voltage. Inspired by *power transmission distribution factors* (PTDF), we introduce sensitivity matrix $\boldsymbol{A} \in \mathbb{R}^{3L\times 3N}$, where L is the number of lines and N is the number of nodes, to map the change of nodal power at each node to the change of line power flow in three-phase system. Note that the PDN system in this paper is radial, thus, the $\boldsymbol{A}$ can be constructed as:

$$a_{l,i}^{\phi,\phi'} := \begin{cases} 1 & \text{if line } l \text{ of phase } \phi \text{ is the part of the} \\ & \text{path from root to bus } i \text{ at phase } \phi' \\ 0 & \text{otherwise} \end{cases}, \forall l,i,\phi,\phi' \quad \text{(D1)}$$

where $a_{l,i}^{\phi,\phi'}$ indicates the element in column $3(i-1)+\phi'$ of row $3(l-1)+\phi$ of the matrix $\boldsymbol{A}$. Thus, the change of nodal power to the change of each line power flow in three-phase system can be described as:

$$\Delta \boldsymbol{P}_{\boldsymbol{line}} = \boldsymbol{A}\cdot\Delta\boldsymbol{P}, \forall l,\phi \quad \text{(D2)}$$

$$\Delta \boldsymbol{P}_{\boldsymbol{line}} = [\Delta P_1^a;\Delta P_1^b;\Delta P_1^c;...;\Delta P_l^\phi;...;\Delta P_L^a;\Delta P_L^b;\Delta P_L^c] \quad \text{(D3)}$$

$$\Delta \boldsymbol{P} = [\Delta P_1^a;\Delta P_1^b;\Delta P_1^c;...;\Delta P_i^\phi;...;\Delta P_N^a;\Delta P_N^b;\Delta P_N^c] \quad \text{(D4)}$$

where $\Delta \boldsymbol{P}^{\boldsymbol{l}}$ indicates the change vector of active line flow and ΔP_l^ϕ means the active flow change of line l at phase ϕ; $\Delta \boldsymbol{P}$ indicates the change vector of nodal power and ΔP_i^ϕ means the nodal power change of node i at phase ϕ. Thus, for specific line l's active power change at phase ϕ can be calculated as:

$$\Delta P_l^\phi = \boldsymbol{A}_{l,*}^\phi \Delta \boldsymbol{P}, \forall l,\phi \quad \text{(D5)}$$

where $\boldsymbol{A}_{l,*}^\phi \in \mathbb{R}^{1\times 3N}$ means the whole row $3(l-1)+\phi$ of sensitivity matrix $\boldsymbol{A}$. Similarly, the reactive line flow change and the reactive nodal power change should satisfy:

$$\Delta Q_l^\phi = \boldsymbol{A}_{l,*}^\phi \Delta \boldsymbol{Q}, \forall l,\phi \quad \text{(D6)}$$

Thus, the sensitivity matrixes of line flow and voltage to nodal power can be described as:

$$\boldsymbol{JP}_{l,t}^\phi = \frac{\partial P_{l,t}^\phi}{\partial \boldsymbol{S}_t} = [\frac{\partial P_{l,t}^\phi}{\partial \boldsymbol{P}_t}, \frac{\partial P_{l,t}^\phi}{\partial \boldsymbol{Q}_t}] = [\mathbf{A}_{l*}^\phi, \mathbf{0}^{1\times 3N}] \quad \text{(D7)}$$

$$\boldsymbol{JQ}_{l,t}^\phi = \frac{\partial Q_{l,t}^\phi}{\partial \boldsymbol{S}_t} = [\frac{\partial Q_{l,t}^\phi}{\partial \boldsymbol{P}_t}, \frac{\partial Q_{l,t}^\phi}{\partial \boldsymbol{Q}_t}] = [\mathbf{0}^{1\times 3N}, \mathbf{A}_{l*}^\phi] \quad \text{(D8)}$$

where $\boldsymbol{JP}_{l,t}^\phi$ and $\boldsymbol{JQ}_{l,t}^\phi$ indicate the sensitivity matrixes of active and reactive line flow (line l at phase ϕ) to nodal power. Collecting the sensitivity matrixes of individual lines, the following coefficient matrixes can be formulated as:

$$\boldsymbol{JP} = \left[\boldsymbol{JP}_1^a;\boldsymbol{JP}_1^b;\boldsymbol{JP}_1^c;...\boldsymbol{JP}_l^\phi;...;\boldsymbol{JP}_L^a;\boldsymbol{JP}_L^b;\boldsymbol{JP}_L^c\right] \quad \text{(D9)}$$

$$\boldsymbol{JQ} = \left[\boldsymbol{JQ}_1^a;\boldsymbol{JQ}_1^b;\boldsymbol{JQ}_1^c;...\boldsymbol{JQ}_l^\phi;...;\boldsymbol{JQ}_L^a;\boldsymbol{JQ}_L^b;\boldsymbol{JQ}_L^c\right] \quad \text{(D10)}$$

The original voltage drop of line l at phase ϕ can be expressed as:

$$u_i^\phi - u_j^\phi = 2(\hat{\boldsymbol{R}}_{\boldsymbol{l}}\cdot\boldsymbol{P}_{\boldsymbol{l}} + \hat{\boldsymbol{X}}_{\boldsymbol{l}}\cdot\boldsymbol{Q}_{\boldsymbol{l}}), i=o(l), j=r(l) \quad \text{(D11)}$$

where $\hat{\boldsymbol{R}}_{\boldsymbol{l}}$ and $\hat{\boldsymbol{X}}_{\boldsymbol{l}}$ are the real part and the imaginary part of the transformed sequence impedance matrix $\hat{\boldsymbol{Z}}_{\boldsymbol{l}}$ of line l. We can find that the voltage drop of line sides is just related to the line flow. Since the root voltage, i.e., substation voltage, is always fixed as the reference voltage. Thus, a certain nodal voltage change such as node i is related to all the line flow changes of the path from root to node i. Thus, the nodal voltage change of node i at phase ϕ can be calculated as:

$$\Delta u_i^\phi = -2\cdot[\mathbf{A}_{*i}^\phi]^\top\cdot(\hat{\boldsymbol{R}}\cdot\Delta\boldsymbol{P}_{\boldsymbol{line}} + \hat{\boldsymbol{X}}\cdot\Delta\boldsymbol{Q}_{\boldsymbol{line}}) \quad \text{(D12)}$$

$$\hat{\boldsymbol{R}} = diag\{\hat{\boldsymbol{R}}_1,...,\hat{\boldsymbol{R}}_l,...,\hat{\boldsymbol{R}}_L\} \quad \text{(D13)}$$

$$\hat{\boldsymbol{X}} = diag\{\hat{\boldsymbol{X}}_1,...,\hat{\boldsymbol{X}}_l,...,\hat{\boldsymbol{X}}_L\} \quad \text{(D14)}$$

where $\mathbf{A}_{*i}^\phi$ indicates the column $3(i-1)+\phi$ of matrix $\boldsymbol{A}$; $\hat{\boldsymbol{R}}$ and $\hat{\boldsymbol{X}}$ are the matrixes constructed from the transformed sequence impedance matrix of each line as shown in (E13) and (E14). Thus, the sensitivity matrix of nodal voltage (node i at phase ϕ) to nodal power can be derived as:

$$\boldsymbol{JV}_{i,t}^\phi = \frac{\partial u_{i,t}^\phi}{\partial \boldsymbol{S}_t} = -2[\mathbf{A}_{*i}^\phi]^\top\cdot\left[\hat{\boldsymbol{R}}\cdot\boldsymbol{JP} + \hat{\boldsymbol{X}}\cdot\boldsymbol{JQ}\right] \quad \text{(D15)}$$

Collecting the sensitivity matrixes of individual nodal voltage, the following coefficient matrixes can be formulated as:

$$\boldsymbol{JV} = \left[\boldsymbol{JV}_1^a;\boldsymbol{JV}_1^b;\boldsymbol{JV}_1^c;...\boldsymbol{JV}_i^\phi;...;\boldsymbol{JV}_N^a;\boldsymbol{JV}_N^b;\boldsymbol{JV}_N^c\right] \quad \text{(D16)}$$

APPENDIX E: PROOF FOR PROPOSITION 2

Through proposed affine policy and balance participation factor, the change of nodal power to the change of uncertain net electric load can be depicted in (16). After the sensitivity matrix analysis of whole system, the change of line flow and nodal voltage to the change of nodal power can be described in (19). Thus, the change of line flow and nodal voltage to the change of uncertain net electric load can be derived as below after substituting (16) into (19):

$$\Delta P_l^\phi = \boldsymbol{JP}_{l,t}^\phi\Delta\boldsymbol{S} = \boldsymbol{JP}_{l,t}^\phi\begin{bmatrix}\Delta\boldsymbol{P}\\ \Delta\boldsymbol{Q}\end{bmatrix} = \boldsymbol{JP}_{l,t}^\phi\begin{bmatrix}\boldsymbol{D}-\boldsymbol{B}\\ \boldsymbol{\alpha}\odot\boldsymbol{D}-\boldsymbol{\alpha}\odot\boldsymbol{B}\end{bmatrix}\boldsymbol{\xi} \quad \text{(E1)}$$

$$= \boldsymbol{XP}_{l,t}^\phi\boldsymbol{\xi}, \forall l,\phi$$

$$where\ \boldsymbol{XP}_{l,t}^\phi = \boldsymbol{JP}_{l,t}^\phi\cdot\begin{bmatrix}\boldsymbol{D}-\boldsymbol{B}\\ \boldsymbol{\alpha}\odot\boldsymbol{D}-\boldsymbol{\alpha}\odot\boldsymbol{B}\end{bmatrix}, \forall l,\phi,t \quad \text{(E2)}$$

where $\boldsymbol{\alpha}$ the given power factor vector. Thus, the responding functions of active line flow to nodal net electric load deviation $\boldsymbol{\xi}$ can be written as:

$$\tilde{P}_{l,t}^\phi = P_{l,t}^\phi + \boldsymbol{XP}_{l,t}^\phi\cdot\boldsymbol{\xi}_t, \forall l,\phi,t \quad \text{(E3)}$$

Similarly, the responding functions of reactive line flow and nodal voltage to nodal net electric load deviation $\boldsymbol{\xi}$ can be written as:

$$\tilde{Q}_{l,t}^\phi = Q_{l,t}^\phi + \boldsymbol{XQ}_{l,t}^\phi\cdot\boldsymbol{\xi}_t, \forall l,\phi,t \quad \text{(E4)}$$

$$where\ \boldsymbol{XQ}_{l,t}^{\phi} = \boldsymbol{JQ}_{l,t}^{\phi} \cdot \begin{bmatrix} \boldsymbol{D} - \boldsymbol{B} \\ \boldsymbol{\alpha} \odot \boldsymbol{D} - \boldsymbol{\alpha} \odot \boldsymbol{B} \end{bmatrix}, \forall l, \phi, t \qquad \text{(E5)}$$

$$\tilde{u}_{i,t}^{\phi} = u_{i,t}^{\phi} + \boldsymbol{XV}_{i,t}^{\phi} \cdot \boldsymbol{\xi}_t, \forall i, \phi, t \qquad \text{(E6)}$$

$$where\ \boldsymbol{XV}_{i,t}^{\phi} = \boldsymbol{JV}_{i,t}^{\phi} \cdot \begin{bmatrix} \boldsymbol{D} - \boldsymbol{B} \\ \boldsymbol{\alpha} \odot \boldsymbol{D} - \boldsymbol{\alpha} \odot \boldsymbol{B} \end{bmatrix}, \forall i, \phi, t \qquad \text{(E7)}$$

APPENDIX F: ADDITIONAL REFERENCES

[F1] W. Gan et al., "Coordinated Planning of Transportation and Electric Power Networks With the Proliferation of Electric Vehicles," *IEEE Trans. on Smart Grid*, vol. 11, no. 5, pp. 4005–4016, Sep. 2020.

[F2] L. Affolabi, M. Shahidehpour, F. Rahimi, F. Aminifar, K. Nodehi, and S. Mokhtari, "DSO market for transactive scheduling of electric vehicle charging stations in constrained hierarchical power distribution and urban transportation networks," *IEEE Trans. Transp. Electrif.*, pp. 1-1, 2023.

[F3] S. Peng, X. Lin, J. Tang, K. Xie, F. Ponci, A. Monti, and W. Li, "Probabilistic power flow of AC/DC hybrid grids with addressing boundary issue of correlated uncertainty sources," *IEEE Trans. Sustainable Energy*, vol. 13, no. 3, pp. 1607-1619, 2022.

[F4] S. Peng, J. Tang, and W. Li, "Probabilistic power flow for AC/vsc-mtdc hybrid grids considering rank correlation among diverse uncertainty sources," *IEEE Trans. Power Syst.*, vol. 32, no. 5, pp. 4035-4044, 2017.

[F5] X. Wu, H. Li, X. Wang, and W. Zhao, "Cooperative operation for wind turbines and hydrogen fueling stations with on-site hydrogen production," *IEEE Trans. Sustainable Energy*, vol. 11, no. 4, pp. 2775-2789, 2020.

[F6] H. Wang, Z. Bie, and H. Ye, "Locational marginal pricing for flexibility and uncertainty with moment information," *IEEE Trans. Power Syst.*, vol. 38, no. 3, pp. 2761-2775, 2023.